



RESEARCH ARTICLE

WILEY

Dual closed-loop tracking control for wheeled mobile robots via active disturbance rejection control and model predictive control

Hongjiu Yang¹  | Mingchao Guo² | Yuanqing Xia³  | Zhongqi Sun³

¹Tianjin Key Laboratory, School of Electrical and Information Engineering of Process Measurement and Control, Tianjin University, Tianjin, China

²Institute of Electrical Engineering, Yanshan University, Qinhuangdao, China

³School of Automation, Beijing Institute of Technology, Beijing, China

Correspondence

Hongjiu Yang, Tianjin Key Laboratory of Process Measurement and Control, School of Electrical and Information Engineering, Tianjin University, Tianjin 300072, China.
Email: yanghongjiu@tju.edu.cn

Funding information

National Natural Science Foundation of China, Grant/Award Number: 61973230, 61573301 and 61733012

Summary

A dual closed-loop tracking control is proposed for a wheeled mobile robot based on active disturbance rejection control (ADRC) and model predictive control (MPC). In the inner loop system, the ADRC scheme with an extended state observer (ESO) is proposed to estimate and compensate external disturbances. In the outer loop system, the MPC strategy is developed to generate a desired velocity for the inner loop dynamic system subject to a diamond-shaped input constraint. Both effectiveness and stability analysis are given for the ESO and the dual closed-loop system, respectively. Simulation results demonstrate the performances of the proposed control scheme.

KEYWORDS

active disturbance rejection control, dual closed-loop control, model predictive control, tracking control, wheeled mobile robot

1 | INTRODUCTION

In recent decades, research works on a wheeled mobile robot (WMR) have been widely investigated owing to its broad applications in many fields.^{1–3} The main theoretical and practical challenges for trajectory tracking control of the WMR are model uncertainties, disturbances, and system constraints. So far, many techniques have been developed for tracking control of the WMR. Purely kinematic controllers are designed based on the assumption of perfect velocity tracking in the works of de Wit and Sordalen⁴ and Xiao et al.⁵ However, it is usually not practical.⁶ Therefore, some researchers changed the object from the design of kinematic controller to the integration design of kinematic controller and dynamic controller. The work of Huang et al.⁷ advocated both kinematic controller and adaptive torque controller in the presence of external disturbances and unknown parameters. Lin and Yang⁸ presented an adaptive critic motion control to autonomously generate the control ability by learning through trials. Song et al.⁹ studied a tracking control problem of multiple-input–multiple-output nonaffine systems based on the readily computable deep-rooted information. In the work of Saradagi et al.,¹⁰ multitime scale implementation methods were used to achieve multiobjective tasks for a nonholonomic mobile inverted pendulum robot under a two-loop control architecture. Through the aforementioned analysis, a dual closed-loop control structure is considered to address the problem of both tracking control and the external disturbances for the WMR. However, most papers did not deal with the input constraints, such as actuator saturation. Therefore, a design of the dual closed-loop control structure is an urgent demand to handle both external disturbances and constraints for the WMR system.

In order to deal with the external disturbances, several elegant approaches have been proposed, including disturbance observer,¹¹ adaptive PI control,¹² and extended state observer (ESO).¹³ Due to a promising feature that ESO requires the least amount of plant information, a control scheme of active disturbance rejection control (ADRC) with an ESO has become more and more popular in recent years. The ADRC technology advocated by Han¹⁴ is a kind of robust control to estimate and compensate the internal and external disturbances and uncertainties. In the work of Tian and Gao,¹⁵ the authors proposed a frequency domain stability analysis of linear ADRC with parameter perturbations of linear plants. A tracking control by the linear ADRC method was presented for a lateral motion of autonomous land vehicle in the work of Xia et al.¹⁶ The linear ADRC was used in the aforementioned two papers. As a matter of fact, the linear ADRC is competent in most occasions. However, if there is a need to pursue more efficiency, the nonlinear ADRC is worthy of consideration.¹⁷ Then, a nonlinear ADRC scheme for a magnetic rodless cylinder was proposed in the work of Zhao et al.,¹⁸ where a self-stable region theory was used to prove the convergence of the nonlinear ESO. In the work of Wu and Chen,¹⁹ stability analysis of a nonlinear ADRC was performed via a describing function method. However, the limitations of the describing function method are complicated and are not universal to transform the nonlinear ADRC system into a system suitable for the describing function method. In the work of Zhao and Guo,²⁰ the convergence theory of a fractional power nonlinear ESO was provided with an explicit error estimation. However, the effectiveness of the linear or nonlinear ESO in most works is presented based on the third-order or higher-order ESO. Hence, a novel convergence theory for the second order nonlinear ESO is designed in this paper.

Model predictive control (MPC) is an effective approach to deal with the constrained control problems. An optimal control input sequence is obtained by solving a finite horizon optimization control problem online at each sampling instant. The first portion of the sequence is applied to the system at each actuator update period.²¹ An MPC scheme with softening constraints was applied to a WMR for trajectory tracking in the work of Yang et al.,²² in which the phenomena of control jump and infeasible solutions were avoided. A robust MPC method by using neural network-based optimization was developed to stabilize a constrained WMR in the work of Xiao et al.²³ However, a terminal-state penalty term in a cost function was not considered such that stability of the system was not guaranteed due to the use of a finite receding horizon.²¹ Therefore, the terminal-state penalty term was constructed on a terminal region to ensure the stability of a WMR system in the work of Gu and Hu.²⁴ In the work of Ma et al.,²⁵ the authors combined MPC and ESO to solve the trajectory tracking problem for an unmanned quadrotor helicopter with disturbances. However, the theoretical proof of the recursive feasibility for the MPC scheme was not given. In addition, most works assume that the control input constraint is independent, which is not able to model the mechanic constraint accurately in practice. Hence, a type of diamond-shaped input constraint deduced from the mechanic model of a WMR was designed in the work of Chen and Jia.²⁶ Following the aforementioned work,²⁶ a receding horizon tracking control problem for a WMR subject to diamond-shaped input constraint was investigated, and the recursive feasibility was guaranteed by developing a positively invariant terminal-state region and a terminal controller in the work of Sun and Xia.²⁷ Motivated by the analysis earlier, an MPC scheme is proposed to address the trajectory tracking problem for the WMR subject to a diamond-shaped input constraint. Moreover, recursive feasibility of the MPC scheme and stability of the WMR system are guaranteed in this paper.

The remainder of this paper is organized as follows. In Section 2, both kinematic model and dynamic model as well as a dual closed-loop control structure are introduced for the WMR. In Section 3, a dynamic controller based on the ADRC technology is proposed. Section 4 details the design procedure of the MPC scheme. Simulation results are exhibited in Section 5. Finally, we summarize our work in Section 6.

Notation . In the following section, if not explicitly stated, matrices are assumed to have compatible dimensions. $\|x\| \triangleq \sqrt{x^T x}$ is the Euclidean norm. P -weighted norm is denoted as $\|x\|_P \triangleq \sqrt{x^T P x}$, where P is a positive definite matrix with appropriate dimension. The signal $\text{diag}\{x_1 \ x_2 \ \dots \ x_n\}$ denotes the diagonal matrix with entries $x_1, x_2, \dots, x_n \in \mathbb{R}$. A nonlinear function $\text{fal}(\cdot)$ used in ADRC theory is defined as follows:

$$\text{fal}(e, \sigma, \delta) = \begin{cases} e/\delta^{(1-\sigma)} & |e| \leq \delta \\ |e|^\sigma \text{sign}(e) & |e| > \delta, \end{cases}$$

where e is a real number, both $0 < \sigma < 1$ and $\delta > 0$ are two given parameters, respectively.

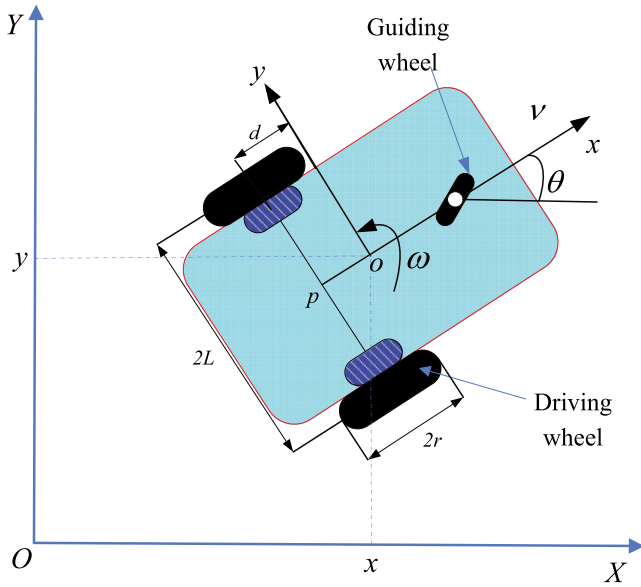


FIGURE 1 A wheeled mobile robot [Colour figure can be viewed at wileyonlinelibrary.com]

2 | WMR MODEL AND CONTROL STRUCTURE

2.1 | Kinematic model

A WMR shown in Figure 1 is a typical nonholonomic mechanical system. In Figure 1, $\{O, X, Y\}$ is a global coordinate frame attached to the ground and $\{o, x, y\}$ is a local coordinate frame attached to the WMR, where o is the mass center and p is the geometrical center. d represents the distance between o and p . The half length of the wheelbase and the radius of motorized wheels are labeled with L and r , respectively. The kinematic model of the real WMR is written as⁷

$$\dot{q} = f(q, u_c) = \begin{bmatrix} \cos \theta & -d \sin \theta \\ \sin \theta & d \cos \theta \\ 0 & 1 \end{bmatrix} \begin{bmatrix} v_c \\ \omega_c \end{bmatrix}, \quad (1)$$

$3 \times 1 = 3 \times 2 + 2 \times 1$

where $q = [\xi \ \theta]^T$ denotes the state with coordinate $\xi = [x \ y]^T$ of point o in the global coordinate frame and orientation θ of the local coordinate frame measured from X axis, and $u_c = [v_c \ \omega_c]^T$ is the control input vector with linear velocity v_c and angular velocity ω_c , respectively.

The purpose is to design a kinematic controller for the WMR to track a reference trajectory. Then, denote a virtual WMR in the global coordinate frame $\{O, X, Y\}$ as follows:

$$\dot{q}_r = f(q_r, u_r) = \begin{bmatrix} \cos \theta_r & -d \sin \theta_r \\ \sin \theta_r & d \cos \theta_r \\ 0 & 1 \end{bmatrix} \begin{bmatrix} v_r \\ \omega_r \end{bmatrix},$$

where $q_r = [\xi_r \ \theta_r]^T$ is the posture of the virtual WMR.

For the tracking objective, we define $q_e(t) = [\xi_e \ \theta_e]^T$ as the state-following error, which is defined with respect to the local coordinate frame $\{o \ x \ y\}$ fixed on the WMR and is given by

$$\xi_e = R(\theta)(\xi_r - \xi), \quad (2)$$

$$\theta_e = \theta_r - \theta, \quad (3)$$

where

$$\xi_e = [x_e \ y_e]^T, \quad R(\theta) = \begin{bmatrix} \cos(\theta) & \sin(\theta) \\ -\sin \theta & \cos \theta \end{bmatrix}.$$

By taking the derivative of ξ_e in (2) as in the work of Huang et al.,⁷ the position tracking error system is given as follows:

$$\dot{\xi}_e = \begin{bmatrix} 0 & \omega_c \\ -\omega_c & 0 \end{bmatrix} \begin{bmatrix} x_e \\ y_e \end{bmatrix} + u_e, \quad (4)$$

where

$$u_e = \begin{bmatrix} u_{e1} \\ u_{e2} \end{bmatrix} = \begin{bmatrix} -v_c + v_r \cos \theta_e - d\omega_r \sin \theta_e \\ -d\omega_c + v_r \sin \theta_e + d\omega_r \cos \theta_e \end{bmatrix} \quad (5)$$

is named as a **kinematic error controller**.

运动学误差控制器

2.2 | Dynamic model

The **dynamic model of the WMR** is described as

$$M(q)\ddot{q} + C_m(q, \dot{q})\dot{q} + F(\dot{q}) + \tau_d = B(q)\tau - A^T(q)\lambda, \quad (6)$$

where $M(q)$ is the symmetric and positive-definite inertia matrix; $C_m(q, \dot{q})$ represents the centripetal and coriolis matrix; $F(\dot{q})$ and τ_d denote the surface friction and the bounded unknown disturbances, respectively; $B(q)$ is the input transformation matrix; $A(q)$ is the matrix associated with constraints; λ is the Lagrange multiplier; and τ represents the control torque generated by the left and right DC motor, respectively. The parameter matrices in (6) are given as follows:

$$M(q) = \begin{bmatrix} m & 0 & md \sin \theta \\ 0 & m & -md \cos \theta \\ md \sin \theta & -md \cos \theta & I_0 \end{bmatrix}, \quad B(q) = \frac{1}{r} \begin{bmatrix} \cos \theta & \cos \theta \\ \sin \theta & \sin \theta \\ L & -L \end{bmatrix}, \quad A^T(q) = \begin{bmatrix} -\sin \theta \\ \cos \theta \\ -d \end{bmatrix},$$

$$\tau = \begin{bmatrix} \tau_l \\ \tau_r \end{bmatrix}, \quad C_m(q, \dot{q}) = \begin{bmatrix} md\dot{\theta}^2 \cos \theta & md\dot{\theta}^2 \sin \theta & 0 \end{bmatrix}^T, \quad \lambda = -m(\dot{x} \cos \theta + \dot{y} \sin \theta)\dot{\theta},$$

where parameters m and I_0 are the mass and the moment of inertia for the WMR, respectively.

Let

$$S(q) = \begin{bmatrix} \cos \theta & -d \sin \theta \\ \sin \theta & d \cos \theta \\ 0 & 1 \end{bmatrix}$$

and, by multiplying $S^T(q)$ on both sides of the dynamic model (6), it follows that

$$\dot{\eta} = \tilde{M}^{-1}(q)\tilde{\tau} + \varpi, \quad (7)$$

where

$$\tilde{M}(q) = \begin{bmatrix} m & 0 \\ 0 & I_0 - md^2 \end{bmatrix}, \quad \tilde{\tau} = \begin{bmatrix} \tau_1 \\ \tau_2 \end{bmatrix} = \frac{1}{r} \begin{bmatrix} 1 & 1 \\ L & -L \end{bmatrix} \tau,$$

$$\eta = [v \ \omega]^T, \quad \varpi = \begin{bmatrix} \varpi_1 \\ \varpi_2 \end{bmatrix} = \tilde{M}^{-1}(q)S(q)(F(\dot{q}) + \tau_d),$$

with $F(q) = [f_1 \ f_2 \ f_3]^T$ and $\tau_d = [\tau_{d1} \ \tau_{d2} \ \tau_{d3}]^T$. $\tilde{\tau}$ is the control law that needs to design in the following section. $\eta = [v \ \omega]^T$ is the real linear velocity and angular velocity to drive the WMR. The variable ϖ is regarded as the total external disturbances. In addition, assume that ϖ and its derivative are bounded.

2.3 | Dual closed-loop control structure

A general dual closed-loop control structure for the WMR is illustrated in Figure 2. The controllers consists of two parts: a kinematic controller and a dynamic controller. The kinematic controller is proposed to generate the desired velocity u_c for the inner loop system. And the dynamic controller is designed to conduct the motion of the WMR so as to track the desired velocity u_c . The ESO is designed to estimate ϖ . The solutions of the kinematic controller and the dynamic controller will be shown in the following section.

Proof. First, we consider the case $\epsilon > 0$. Based on the conditions $e_{21} = e_1$ and $e_{22} = e_2 - \beta_1 e_1$, the estimation error systems (14) and (15) are rewritten as

$$\dot{e}_{21} = e_{22}, \quad (16)$$

$$\dot{e}_{22} = -\beta_2 \text{fal}(e_{21}, \sigma, \delta) - \beta_1 e_{22} - \epsilon. \quad (17)$$

Construct a Lyapunov function

$$V_1 = \int_0^{e_{21}} 2\beta_2 \text{fal}(\zeta, \sigma, \delta) d\zeta + e_{22}^2. \quad (18)$$

There exists a $\gamma \in [0, e_{21}]$ such that the Lyapunov function (18) satisfies the following equation:

$$\begin{aligned} V_1 &= \int_0^{e_{21}} 2\beta_2 \text{fal}(\zeta, \sigma, \delta) d\zeta + e_{22}^2 \\ &= 2\beta_2 \text{fal}(\gamma, \sigma, \delta) e_{21} + e_{22}^2. \end{aligned}$$

Due to $\beta_2 > 0$ and the function $\text{fal}(\cdot)$ being an odd function, one has

$$V_1 = 2\beta_2 \text{fal}(\gamma, \sigma, \delta) e_{21} + e_{22}^2 > 0.$$

The derivative of (18) is given by

$$\begin{aligned} \dot{V}_1 &= 2e_{22}\beta_2 \text{fal}(e_{21}, \sigma, \delta) + 2e_{22}[-\beta_2 \text{fal}(e_{21}, \sigma, \delta) - \epsilon - \beta_1 e_{22}] \\ &= -2e_{22}(\beta_1 e_{22} + \epsilon). \end{aligned}$$

The positive gain β_1 is set such that inequality $|e_{22}| > \frac{\epsilon}{\beta_1}$ is satisfied, then \dot{V}_1 is negative definite.

Note that the analysis process under condition $\epsilon < 0$ is similar to that under $\epsilon > 0$. That is, if inequality $|e_{22}| > -\frac{\epsilon}{\beta_1}$ is met under condition $\epsilon < 0$, $\dot{V}_1 < 0$ holds.

In conclusion, if inequality $|e_{22}| > \frac{|\epsilon|}{\beta_1}$ is satisfied under the positive gain β_1 , \dot{V}_1 is negative definite. Furthermore, the formula $\dot{V}_1 = 0$ holds if and only if e_{22} equals to zero. Hence, the error systems (16) and (17) are convergent, and the observations z_1 and z_2 converge to the actual values x_1 and x_2 , respectively. \square

In the next section, we will design a nonlinear state error feedback controller to conduct the motion of the WMR so as to track the desired velocity v_c .

3.2 | Design of nonlinear state error feedback controller

An error signal $\tilde{\eta}_1$ relative to the desired velocity v_c and the ESO z_1 is defined as follows:

$$\tilde{\eta}_1 = v_c - z_1. \quad (19)$$

The nonlinear state error feedback controller τ_1 is constituted as

$$\tau_1 = k_{\tau_1} \text{fal}(\tilde{\eta}_1, \sigma, \delta) - z_2/b_0, \quad (20)$$

where k_{τ_1} is an adjustable gain, and z_2/b_0 is a compensation for systems (10) and (11). Note that the total gains of the dynamic controller for systems (8) and (9) are labeled with $k_r = \text{diag}\{k_{\tau_1} \ k_{\tau_2}\}$. The inner loop error s_1 between the desired linear velocity v_c and the real linear velocity v is presented as

$$s_1 = v_c - v. \quad (21)$$

The derivative of s_1 is given by

$$\dot{s}_1 = \dot{v}_c - x_2 - b_0 \tau_1. \quad (22)$$

From Equation (21) and the estimation error $e_1 = z_1 - v$, Equation (19) becomes

$$\tilde{\eta}_1 = s_1 - e_1.$$

Substituting Equation (20) into Equation (22) yields

$$\dot{s}_1 = \dot{\eta}_1 - k_{\tau_1} \text{fal}(\tilde{\eta}_1, \sigma, \delta) + e_2.$$

Stability of the inner loop system is analyzed in the following theorem.

Theorem 2. Consider the inner loop error system (21) with the nonlinear state error feedback controller (20). Construct a Lyapunov function V_2 . If there exists a positive coefficient k_{τ_1} such that the derivative of the Lyapunov function V_2 is less than zero, the inner loop error system (21) is convergent. That is, the real linear velocity v converges to the desired linear velocity v_c .

Proof. Choose a Lyapunov function as follows:

$$V_2 = \frac{1}{2}(s_1 - e_1)^2. \quad (23)$$

Taking the derivative of (23) yields

$$\begin{aligned} \dot{V}_2 &= (s_1 - e_1) (\dot{v}_c - k_{\tau_1} \text{fal}(\tilde{\eta}_1, \sigma, \delta) + e_2 - (e_2 - \beta_1 e_1)) \\ &= -(s_1 - e_1) k_{\tau_1} \text{fal}(\tilde{\eta}_1, \sigma, \delta) + (s_1 - e_1) (\dot{v}_c + \beta_1 e_1) \\ &\leq -k_{\tau_1} \tilde{\eta}_1 \text{fal}(\tilde{\eta}_1, \sigma, \delta) + M, \end{aligned}$$

where $M = \sup[(s_1 - e_1)(\dot{v}_c + \beta_1 e_1)]$ is an upper bound. Since function $\text{fal}(\cdot)$ is a monotonically increasing odd function, the part $\tilde{\eta}_1 \text{fal}(\tilde{\eta}_1, \sigma, \delta)$ is no less than zero. Choose a positive gain k_{τ_1} such that $\dot{V}_2 < 0$ holds. Then, the nonlinear state error feedback controller τ_1 in (20) guarantees the stability of the inner loop system. \square

Remark 1. The ESO is designed to estimate ϖ , which brings in the estimate error e_o inevitably. According to the aforementioned analysis, it is shown that e_o is bounded. In addition, it can be seen that the steady-state error of the inner loop system is bounded from Theorem 2. The two errors from the inner loop system will have an effect on the outer loop system. Defining a transferred error e_t in the outer loop system influenced by the two errors, it is obtained that e_t is bounded.

4 | KINEMATIC CONTROLLER BASED ON MPC SCHEME

In this section, an MPC scheme for the kinematic model is developed. In Section 4.1, some preliminaries are introduced. In Section 4.2, an optimization problem for the MPC strategy is described. Recursive feasibility for the MPC scheme and stability for the outer loop system are given in Sections 4.3 and 4.4, respectively.

4.1 | Preliminaries

We rewrite system (2) in a compact form as

$$\dot{\xi}_e = f(\xi_e, u_e). \quad (24)$$

The WMR is subject to a type of diamond-shaped input constraint satisfying $u_c \in \mathbb{U}_c$, where

$$\mathbb{U}_c = \left\{ [v_c \ \omega_c]^T : \frac{|v_c|}{a} + \frac{|\omega_c|}{b} \leq 1 \right\}, \quad (25)$$

with $b = a/d$. Parameter a in (25) is a known positive constant that presents the maximum linear velocity of the driving wheels.

限制了转向角速度和速度的耦合约束关系

Let h be the sampling period and define $\{t + kh : k \in \mathbb{N}\}$ as a time sequence. The goal of designing kinematic controller is to minimize a cost function given by

$$J(\xi_e(t), u_e(t)) = \int_t^{t+T} L(\xi_e(\zeta|t), u_e(\zeta|t)) d\zeta + g(\xi_e(t+T|t)), \quad (26)$$

where $L(\xi_e(\zeta|t), u_e(\zeta|t)) = \|\xi_e(\zeta|t)\|_P^2 + \|u_e(\zeta|t)\|_R^2$ is the stage cost with the positive definite matrices $P = \text{diag}\{p_1 \ p_2\}$ and $R = \text{diag}\{r_1 \ r_2\}$, respectively; $g(\xi_e(t+T|t)) = \frac{1}{2}\|\xi_e(t+T|t)\|^2$ is the terminal penalty; and T is the prediction horizon.

Remark 2. For the finite horizon optimization control problem, the optimal cost function is designed usually as a finite horizon cost to specify the control performance,^{24,27,28} including a stage cost $L(\xi_e(\zeta|t), u_e(\zeta|t))$ and a terminal penalty $g(\xi_e(t+T|t))$. From the work of Sun and Xia,²⁷ the terminal penalty $g(\xi_e(t+T|t))$ and the terminal region Ω mentioned later are adopted to guarantee stability of the MPC closed loop. Note that P and R are tuning parameters. Large values of P in comparison with R lead to the better position tracking performance, whereas large values of R relative to P reduce the position tracking action and focus on the velocity tracking. It is challengeable to minimize a infinite horizon cost of the nonlinear system. Thus, the terminal penalty $g(\xi_e(t+T|t))$ is given to bound the infinite horizon cost.

Based on the work of Yu et al.,²⁸ two assumptions are introduced as follows.

Assumption 1. $L(\cdot, \cdot) : X \times U \rightarrow \mathbb{R}^1$ is continuous, and $L(0, 0) = 0$ and $L(x, u) > 0$ for all $(x, u) \in X \times U \setminus \{0, 0\}$.

Assumption 2. For system (24), there exist a terminal region Ω , a terminal controller $u_c^L(\zeta|t)$, and a continuously differentiable positive semidefinite function $g(\xi_e)$ such that, for any $\xi_e(\zeta|t) \in \Omega$ over the interval $\zeta \in [t+T, t+h+T]$, it holds that

$$\begin{aligned} \xi_e(\zeta|t+h) &\in \Omega, u_c^L(\zeta|t+h) \in \mathbb{U}_c, \\ \dot{g}(\xi_e(\zeta|t)) + L(\xi_e(\zeta|t), u_e(\zeta|t)) &\leq 0. \end{aligned} \quad (27)$$

The following lemma provides the terminal controller and the corresponding terminal region for system (1).

Lemma 1. For system (1), define $\lambda_r = \frac{\sqrt{2}}{a}|v_r|$ under the assumption of $v_r < \frac{a}{\sqrt{2}}$. If there exist parameters k_i satisfying $k_i \in (\frac{1-\sqrt{1-4r_i p_i}}{2r_i}, \frac{1+\sqrt{1-4r_i p_i}}{2r_i})$ with $r_i p_i < \frac{1}{4}$, $i = 1, 2$, the terminal region is $\Omega = \{\xi_e : k_1|x_e| + k_2|y_e| < a(1 - \lambda_r)\}$ and, accordingly, the terminal controller over the interval $\zeta \in [t+T, t+h+T]$ is shown as follows:

$$u_c^L(\zeta|t) = \begin{bmatrix} v_c^L(\zeta|t) \\ \omega_c^L(\zeta|t) \end{bmatrix} = \begin{bmatrix} k_1 x_e + v_r \cos \theta_e - d\omega_r \sin \theta_e \\ \frac{1}{d}(k_2 y_e + v_r \sin \theta_e + d\omega_r \cos \theta_e) \end{bmatrix}. \quad (28)$$

Proof. First, substituting the terminal controller (28) into the input constraint (25), it is obtained as follows:

$$\begin{aligned} \frac{|v_c^L|}{a} + \frac{|\omega_c^L|}{b} &= \frac{k_1|x_e| + |v_r \cos \theta_e| - |d\omega_r \sin \theta_e|}{a} + \frac{k_2|y_e| + |v_r \sin \theta_e| + |d\omega_r \cos \theta_e|}{a} \\ &\leq \frac{1}{a}(k_1|x_e| + |v_r \cos \theta_e| + |d\omega_r \sin \theta_e| + k_2|y_e| + |v_r \sin \theta_e| + |d\omega_r \cos \theta_e|) \\ &\leq 1 - \lambda_r + \frac{\sqrt{2}}{a}|v_r| \\ &= 1, \end{aligned}$$

which implies $u_c^L \in \mathbb{U}_c$ if $\xi_e \in \Omega$ holds.

Next, choose $g(\xi_e(\varsigma|t))$ as a Lyapunov function. The derivative of $g(\xi_e(\varsigma|t))$ with respect to ς yields

$$\begin{aligned}\dot{g}(\xi_e(\varsigma|t)) &= x_e [y_e \omega + v_r \cos \theta_e - d\omega_r \sin \theta_e - (k_1 x_e + v_r \cos \theta_e - d\omega_r \sin \theta_e)] \\ &\quad + y_e [-x_e \omega + v_r \sin \theta_e + d\omega_r \cos \theta_e - (k_2 y_e + v_r \sin \theta_e + d\omega_r \cos \theta_e)] \\ &= - (k_1 x_e^2 + k_2 y_e^2) \leq 0,\end{aligned}$$

which means that Ω is an invariant set by implementing the terminal controller (28). That is, $\xi_e(\varsigma|t) \in \Omega$ holds for all $\varsigma > t$ once $\xi_e(t|t) \in \Omega$.

Finally, for $\xi_e(\varsigma|t) \in \Omega$, substituting Equations (5) and (28) into Equation (27), it follows that

$$\begin{aligned}\dot{g}(\xi_e(\varsigma|t)) + L(\xi_e(\varsigma|t), u_e(\varsigma|t)) &= x_e \dot{x}_e + y_e \dot{y}_e + p_1 x_e^2 + p_2 y_e^2 + r_1 u_{e1}^2 + r_2 u_{e2}^2 \\ &= - (k_1 x_e^2 + k_2 y_e^2) + p_1 x_e^2 + p_2 y_e^2 + r_1 u_{e1}^2 + r_2 u_{e2}^2 \\ &= (r_1 k_1^2 - k_1 + p_1) x_e^2 + (r_2 k_2^2 - k_2 + p_2) y_e^2.\end{aligned}$$

Since $k_i \in (\frac{1-\sqrt{1-4r_i p_i}}{2r_i}, \frac{1+\sqrt{1-4r_i p_i}}{2r_i})$ with $r_i p_i < \frac{1}{4}$, $i = 1, 2$, inequality $\dot{g}(\xi_e(\varsigma|t)) + L(\xi_e(\varsigma|t), u_e(\varsigma|t)) \leq 0$ holds. Hence, from Assumption 2, Ω is the terminal region and, accordingly, the terminal controller is $u_c^L(\varsigma|t)$ over the interval $\varsigma \in [t + T, t + h + T)$. \square

Lemma 2. *The WMR system (1) is locally Lipschitz relative to q in the domain $u_c \in \mathbb{U}_c$. That is, there is a constant $0 < L_c < \infty$ such that the function values of $f(q, u_c)$ at q_1 and q_2 with the same u_c satisfy $\|f(q_1, u_c) - f(q_2, u_c)\| \leq L_c \|q_1 - q_2\|$.*

Proof. Considering the function values of $f(q, u_c)$ at q_1 and q_2 with the same u_c , it is obtained as follows:

$$\begin{aligned}\|f(q_1, u_c) - f(q_2, u_c)\|^2 &= v_c^2 (\cos \theta_1 - \cos \theta_2)^2 + d^2 \omega_c^2 (\sin \theta_2 - \sin \theta_1)^2 + v_c^2 (\sin \theta_1 - \sin \theta_2)^2 + d^2 \omega_c^2 (\cos \theta_2 - \cos \theta_1)^2 \\ &\leq 2 (v_c^2 + d^2 \omega_c^2) (\theta_1 - \theta_2)^2 \\ &\leq 2 \max_{[v_c, \omega_c]^T \in \mathbb{U}} \{v_c^2 + d^2 \omega_c^2\} (\theta_1 - \theta_2)^2 \\ &= a^2 (\theta_1 - \theta_2)^2.\end{aligned}$$

Therefore, inequality $\|f(q_1, u_c) - f(q_2, u_c)\| \leq a \|q_1 - q_2\|$ holds. That is, the Lipschitz constant L_c is a . \square

4.2 | MPC scheme

At the current time t , the outer loop optimization problem solved online is formulated as follows:

$$\min J(\xi_e(t), u_e(t)), \quad (29)$$

subject to

$$\dot{\xi}_e(\varsigma|t) = f(\xi_e(\varsigma|t), u_e(\varsigma|t)), \quad (30)$$

$$u_c(\varsigma|t) \in \mathbb{U}_c, \quad (31)$$

$$\|\xi_e(\varsigma|t)\| \leq \frac{\rho T}{\varsigma - t}, \quad (32)$$

$$\xi_e(t + T|t) \in \Omega_\varepsilon, \quad (33)$$

where $\varsigma \in [t, t + T)$, $J(\cdot, \cdot)$ is given by (26), $\rho = \frac{ab}{\sqrt{a^2 + b^2}}$, and $\Omega_\varepsilon = \{\xi_e : \|\xi_e\| \leq \varepsilon\}$ is a terminal region with $\varepsilon < \rho$.

An optimal predictive control sequence $u_c^*(t)$ is obtained by solving the optimization problem (29)-(33) over the interval $\varsigma \in [t, t + T)$, ie,

$$u_c^*(t) = [u_c^*(t|t), u_c^*(t + h|t), \dots, u_c^*(t + T|t)]. \quad (34)$$

Although $u_c^*(t)$ is performed over the prediction horizon T , only the first element of Equation (34) over the interval $\varsigma \in [t, t + h)$ is applied to the WMR. Hence, the desired velocity $u_c^*(t)$ and the error trajectory $\xi_e^*(t)$ are described as

$$[v_c(\varsigma) \ \omega_c(\varsigma)]^T = u_c^*(t|t), \quad (35)$$

$$\xi_e(\varsigma) = \xi_e^*(\varsigma|t). \quad (36)$$

Remark 3. Due to Brockett conditions and the work of Kühne et al,²⁹ a WMR with nonholonomic constraints cannot be feedback stabilized through continuously differentiable time-invariant control laws. By using MPC, a discontinuous control law is naturally obtained. In this paper, the optimal cost function value (34) is obtained by solving the optimization problem (29)-(33). The optimal cost function value (34) is discontinuous, which means that the optimal cost function value (34) is not differentiable. In the work of Kühne et al,²⁹ the optimization problem is transformed to a quadratic programming (QP) problem by successive linearization of an error model of the WMR. Since QP problem is a convex problem, it is easy to solve by numerically robust solvers, which leads to global optimal solutions. However, linear (and even successively linearized or time-variant) MPC can be problematic for nonholonomic systems (as the linearization around any fixed point is not controllable and the assumptions for guaranteed stability with stability constraints fail).³⁰ Then, the potential of nonlinear MPC techniques is investigated.^{24,26,28} In the work of Fontes,³¹ a continuous-time MPC framework using a strictly positive intersampling time is argued to be appropriate to use with discontinuous optimal controls and discontinuous feedbacks, which is the same as the outer loop optimization problem (29)-(33).

The MPC scheme is summarized in Algorithm 1.

Algorithm 1 MPC Scheme

Require: J : cost function; t_0 : initial time; t : current time; P and R : weighting matrices; T : prediction horizon

- 1: At the initial time t_0 , choose the weighting matrices P , R and the prediction horizon T in the cost function J . Select gains k_1 and k_2 in the terminal controller (28) and initialize the state $q(t_0) = q(0)$;
 - 2: At the current time t , measure the current state $q(t|t) = q(t)$;
 - 3: Solve the outer loop optimization problem (29)-(33) over the interval $\varsigma \in [t, t + T)$ to obtain the optimal predictive control sequence (34);
 - 4: Apply controller (35) over the interval $\varsigma \in [t, t + h)$;
 - 5: Update the time instant $t = t + h$, go to 2.
-

Recursive feasibility of the MPC scheme and stability of the outer loop system are analyzed in the next the section.

4.3 | Recursive feasibility of the MPC scheme

Recursive feasibility of the MPC scheme implies that the solution space of the outer loop optimization problem (29)-(33) is nonempty at each sampling time instant. The following theorems are given to show the recursive feasibility of the MPC scheme.

Theorem 3. Suppose that, at the current time t , there exists an optimal control sequence $u_c^*(\varsigma|t)$ over the interval $\varsigma \in [t, t + T)$. Applying the desired velocity (35) during $[t, t + h)$, the following results are satisfied at the time instant $t + h$.

- (1) The control sequence $u_c^*(\varsigma|t)$ over the interval $\varsigma \in [t + h, t + T)$ is able to drive the tracking error ξ_e into the region $\Omega_\rho = \{\xi_e : \|\xi_e\| \leq \rho\}$ if e_t is bounded by $\|e_t\| \leq \rho$ with $\rho \leq \frac{e^{\rho T}}{h}(\rho - \epsilon)$.
- (2) The state constraint (32) is satisfied, that is, $\|\xi_e(\varsigma|t + h)\| \leq \frac{\rho T}{\varsigma - t - h}$ over the interval $\varsigma \in [t + h, t + T)$ holds if $\rho > \epsilon \geq \frac{\rho(T-h)}{T}$.

Proof. Apply the control signal (35) to the WMR during $\varsigma \in [t, t+h]$. Based on $q(t) = q^*(t|t)$, Lemma 2, and Grönwall-Bellman inequality, the Euclidean norm of the error between $q(t+h)$ and $q^*(t+h|t)$ is shown as follows:

$$\begin{aligned} \|q(t+h) - q^*(t+h|t)\| &= \left\| q(t) + \int_t^{t+h} f(q(\varsigma), u_c) d\varsigma - q^*(t|t) - \int_t^{t+h} f(q^*(\varsigma|t), u_c^*(t|t)) d\varsigma \right\| \\ &\leq \int_t^{t+h} \|e_t(\varsigma)\| d\varsigma + \int_t^{t+h} \|f(q(\varsigma), u_c^*(t|t)) - f(q^*(\varsigma), u_c^*(t|t))\| d\varsigma \\ &\leq \int_t^{t+h} \|e_t(\varsigma)\| d\varsigma + a \int_t^{t+h} \|q(\varsigma) - q^*(\varsigma|t)\| d\varsigma \\ &\leq e^{ah} \int_t^{t+h} \|e_t(\varsigma)\| d\varsigma. \end{aligned} \quad (37)$$

At the time instant $t+h$, the control sequence $u_c^*(\varsigma|t)$ is applied to the WMR during $\varsigma \in [t+h, t+T]$. Combining with (37) and applying Grönwall-Bellman inequality again, the error between the feasible trajectory $q(\varsigma|t+h)$ and the optimal trajectory $q^*(\varsigma|t)$ is shown as follows:

$$\begin{aligned} &\|q(\varsigma|t+h) - q^*(\varsigma|t)\| \\ &= \left\| q(\varsigma|t+h) + \int_{t+h}^{\varsigma} f(q(s|t+h), \eta^*(s|t)) ds - q^*(t+h|t) - \int_{t+h}^{\varsigma} f(q^*(s|t), \eta^*(s|t)) ds \right\| \\ &\leq e^{a(\varsigma-t)} \int_t^{t+h} \|e_t(\varsigma)\| d\varsigma. \end{aligned}$$

Due to $\|\xi_e(t+T|t+h) - \xi_e^*(t+T|t)\| \leq \|q(t+T|t+h) - q^*(t+T|t)\|$ and $\|e_t(\varsigma)\| \leq \rho$, then, at the time instant $t+T$, one has

$$\|\xi_e(t+T|t+h)\| \leq \|\xi_e^*(t+T|t)\| + \rho h e^{aT}. \quad (38)$$

Substituting the conditions $\|\xi_e^*(t+T|t)\| \leq \varepsilon$ and $\rho < \frac{e^{-aT}}{h}(\rho - \varepsilon)$ into (38), it follows that

$$\|\xi_e(t+T|t+h)\| \leq \rho, \quad (39)$$

which implies $\xi_e(t+T|t+h) \in \Omega_\rho$. That is, the first conclusion in Theorem 3 is satisfied.

Next, over the interval $\varsigma \in [t+h, t+T]$, inequality (38) is rewritten as

$$\|\xi_e(\varsigma|t+h)\| \leq \|\xi_e^*(\varsigma|t)\| + \rho h e^{aT}.$$

Due to the conditions $\rho \leq \frac{e^{-aT}}{h}(\rho - \varepsilon)$, $\|\xi_e^*(\varsigma|t)\| \leq \frac{\rho T}{\varsigma-t}$ and $\rho > \varepsilon \geq \frac{\rho(T-h)}{T}$, it follows that

$$\|\xi_e^*(\varsigma|t+h)\| \leq \frac{\rho T}{\tau - t_k} + (\rho - \varepsilon) \leq \frac{\rho T}{\tau - t_k} + \frac{h\rho T}{(\varsigma - t - h)(\varsigma - t)} \leq \frac{\rho T}{\varsigma - t - h}.$$

Thus, the second conclusion holds. \square

Theorem 4. If $\xi_e(t+T) \in \Omega_\rho$ and $2kh \geq \ln \frac{\rho}{\varepsilon}$ with $k = \min\{k_1, k_2\}$, the terminal controller $u_c^L(\varsigma|t+h)$ over the interval $\varsigma \in [t+T, t+h+T]$ is able to drive the tracking error ξ_e into Ω_ε in one step, ie, $\xi_e(t+h+T|t+h) \in \Omega_\varepsilon$.

Proof. At the time instant $t+T$, the control signal is switched to $u_c^L(\varsigma|t+h)$. Then, during $\varsigma \in [t+T, t+h+T]$, the derivative of $g(\xi_e(\varsigma|t+h))$ with respect to ς is shown as

$$\begin{aligned} \dot{g}(\xi_e(\varsigma|t+h)) &= -(k_1 x_e^2 + k_2 y_e^2) \\ &\leq -2kg(\xi_e(\varsigma|t+h)), \end{aligned} \quad (40)$$

where $k = \min\{k_1, k_2\}$.

Solving inequality (40) yields

$$\|\xi_e(\varsigma|t+h)\| \leq \|\xi_e(t+T|t+h)\| e^{-2k(\varsigma-(t+T))}. \quad (41)$$

At the terminal time instant $\varsigma = t+h+T$, inequality (41) results in

$$\|\xi_e(t+h+T|t+h)\| \leq \|\xi_e(t+T|t+h)\| e^{-2kh}. \quad (42)$$

Moreover, substituting (39) and the condition $2kh \geq \ln \frac{\rho}{\varepsilon}$ into (42), it is obtained that

$$\|\xi_e(t+h+T|t+h)\| \leq \varepsilon. \quad (43)$$

Therefore, the terminal controller $u_c^L(\varsigma|t+h)$ is able to drive the tracking error into the terminal region Ω_ε . \square

4.4 | Stability analysis of the outer loop system

Theorem 5. *For the trajectory tracking problem of the outer loop system, the position tracking error system is given by (4). Suppose the WMR system is controlled by (35) and all the conditions in Theorems 3 and 4 are satisfied, then the position tracking error system (4) is asymptotically convergent.*

Proof. Considering the difference of the cost function $J(\xi_e^*(t), u_e^*(t))$ at t and $t+h$, one has

$$V_3(t) = J(\xi_e^*(t+h), u_e^*(t+h)) - J(\xi_e^*(t), u_e^*(t)) \leq J(\xi_e(t+h), u_e(t+h)) - J(\xi_e^*(t), u_e^*(t)). \quad (44)$$

For convenience, $V_3(t)$ is divided into three parts such that $V_3 = V_{31} + V_{32} + V_{33}$, where $V_{31}(t) = -\int_t^{t+h} [\|\xi_e^*(\varsigma|t)\|_p^2 + \|u_e^*(\varsigma|t)\|_R^2] d\varsigma$, $V_{32}(t) = \int_{t+h}^{t+T} [\|\xi_e(\varsigma|t+h)\|_p^2 - \|\xi_e^*(\varsigma|t)\|_p^2] d\varsigma$, and $V_{33}(t) = \int_{t+T}^{t+h+T} [\|\xi_e(\varsigma|t+h)\|_p^2 - \|u_e(\varsigma|t+h)\|_R^2] d\varsigma + \frac{1}{2} \|\xi_e(t+h+T|t+h)\|^2 - \frac{1}{2} \|\xi_e^*(t+T|t)\|^2$.

First, consider $V_{31}(t)$, it is easy to obtain the following inequality:

$$\begin{aligned} V_{31}(t) &= -\int_t^{t+h} [\|\xi_e^*(\varsigma|t)\|_p^2 + \|u_e^*(\varsigma|t)\|_R^2] d\varsigma \\ &\leq -\int_t^{t+h} \|\xi_e^*(\varsigma|t)\|_p^2 d\varsigma. \end{aligned} \quad (45)$$

Next, for $V_{32}(t)$, it can be rewritten as

$$\begin{aligned} V_{32}(t) &= \int_{t+h}^{t+T} [\|\xi_e(\varsigma|t+h)\|_p^2 - \|u_e(\varsigma|t+h)\|_R^2] d\varsigma + \frac{1}{2} \|\xi_e(t+h+T|t+h)\|^2 \\ &\quad - \frac{1}{2} \|\xi_e^*(t+T|t)\|^2 + \frac{1}{2} \|\xi_e(t+T|t+h)\|^2 - \frac{1}{2} \|\xi_e(t+T|t+h)\|^2. \end{aligned} \quad (46)$$

Integrating (27) from $t+T$ to $t+h+T$ yields

$$\int_{t+T}^{t+h+T} [\|\xi_e(\varsigma|t+h)\|_p^2 + \|u_e(\varsigma|t+h)\|_R^2] d\varsigma \leq \frac{1}{2} \|\xi_e(t+T|t+h)\|^2 + \frac{1}{2} \|\xi_e(t+h+T|t+h)\|^2. \quad (47)$$

Substituting (47) into (46) and using the triangle inequality, it follows that

$$\begin{aligned} V_{32}(t) &\leq \frac{1}{2} \|\xi_e(t+T|t+h)\|^2 - \frac{1}{2} \|\xi_e^*(t+T|t)\|^2 \\ &\leq \frac{1}{2} (\|\xi_e(t+T|t+h) - \xi_e^*(t+T|t)\|)(\|\xi_e(t+T|t+h)\| + \|\xi_e^*(t+T|t)\|). \end{aligned} \quad (48)$$

From (39) and (43), inequality (48) results in

$$V_{32}(t) \leq \frac{1}{2}e^{aT}(\varepsilon + \rho) \int_t^{t+h} \|e_t(\varsigma)\| d\varsigma. \quad (49)$$

Finally, by using the difference square formula and the triangle inequality, $V_{33}(t)$ is calculated as follows:

$$\begin{aligned} V_{33}(t) &\leq \int_{t+h}^{t+T} (\|\xi_e^*(\varsigma|t+h) - \xi_e^*(\varsigma|t)\|_P) (\|\xi_e^*(\varsigma|t+h)\|_P - \|\xi_e^*(\varsigma|t)\|_P) d\varsigma \\ &\leq \int_{t+h}^{t+T} \left[p^2 e^{a(\varsigma-t)} \left(\int_t^{t+h} \|e_t(\varsigma)\| d\varsigma \right) \left(2\|\xi_e^*(\varsigma|t)\| + \int_t^{t+h} \|e_t(\varsigma)\| d\varsigma e^{a(\varsigma-t)} \right) \right] d\varsigma \\ &= \int_{t+h}^{t+T} \left[2p^2 e^{a(\varsigma-t)} \left(\int_t^{t+h} \|e_t(\varsigma)\| d\varsigma \right) \|\xi_e^*(\varsigma|t)\| + p^2 e^{2a(\varsigma-t)} \left(\int_t^{t+h} \|e_t(\varsigma)\| d\varsigma \right)^2 \right] d\varsigma \\ &\leq \int_t^{t+h} \|e_t(\varsigma)\| d\varsigma \int_{t+h}^{t+T} 2p^2 e^{a(\varsigma-t)} \|\xi_e^*(\varsigma|t)\| d\varsigma + \frac{p^2}{2a} (e^{2aT} - e^{2ah}) \left(\int_t^{t+h} \|e_t(\varsigma)\| d\varsigma \right)^2 \\ &\leq \frac{2p^2 \rho}{\sqrt{2a}} (e^{2aT} - e^{2ah})^{\frac{1}{2}} \left(\int_{t+h}^{t+T} \|\xi_e^*(\varsigma|t)\|^2 d\varsigma \right)^{\frac{1}{2}} \int_t^{t+h} \|e_t(\varsigma)\| d\varsigma \\ &\quad + \frac{p^2}{2a} (e^{2aT} - e^{2ah}) \left(\int_t^{t+h} \|e_t(\varsigma)\| d\varsigma \right)^2. \end{aligned}$$

Combining with constraint (32) yields

$$V_{33}(t) \leq \frac{2p^2 \rho}{\sqrt{2a}} \left(\frac{T^2}{h} - T \right)^{\frac{1}{2}} (e^{2aT} - e^{2ah})^{\frac{1}{2}} \int_t^{t+h} \|e_t(\varsigma)\| d\varsigma + \frac{p^2}{2a} (e^{2aT} - e^{2ah}) \left(\int_t^{t+h} \|e_t(\varsigma)\| d\varsigma \right)^2. \quad (50)$$

In conclusion, collecting the results of (45), (49), and (50), it follows that

$$\begin{aligned} V_3 &\leq - \int_t^{t+h} \|\xi_e^*(\varsigma|t)\|_P^2 d\varsigma + \frac{1}{2}e^{aT}(\varepsilon + \rho) \int_t^{t+h} \|e_t(\varsigma)\| d\varsigma + \frac{2p^2 \rho}{\sqrt{2a}} \left(\frac{T^2}{h} - T \right)^{\frac{1}{2}} (e^{2aT} - e^{2ah})^{\frac{1}{2}} \\ &\quad \cdot \int_t^{t+h} \|e_t(\varsigma)\| d\varsigma + \frac{p^2}{2a} (e^{2aT} - e^{2ah}) \left(\int_t^{t+h} \|e_t(\varsigma)\| d\varsigma \right)^2. \end{aligned}$$

Due to $\lim_{t \rightarrow \infty} \int_t^{t+h} \|e_t(\varsigma)\| d\varsigma = 0$ from Theorems 1 and 2, then the position tracking error system (2) is asymptotically convergent. \square

5 | SIMULATION RESULTS

In this section, a reference trajectory tracking simulation is carried out to verify the effectiveness and robustness of the proposed scheme. A comparative simulation with our previous work²² is implemented to verify the performance of trajectory tracking. In addition, parallel parking trajectory tests are presented to show the regulation performance. The structure parameters of the WMR are borrowed from the work of Huang et al,⁷ which are given as $m = 4$ kg, $L = 0.3$ m, $r = 0.1$ m, $d = 0.25$ m, and $I_0 = 2.5$ kg · m².

In this paper, the nonlinear MPC optimization problem (29)-(33) is proposed for the outer loop. Recursive feasibility of the MPC scheme and stability of the WMR system are given, respectively. As for solving the optimization problem, several algorithms are used to find numerical solutions of the nonlinear MPC, such as interior point method³² and branch-and-bound optimization.³³ In this paper, the nonlinear MPC optimization problem (29)-(33) is transcribed by the Imperial College London Optimal Control Software,³⁴ 1.2 version, and solved by the Nonlinear Programming solver Interior Point OPTimizer,³² 3.11.8 version.

5.1 | Trajectory tracking test

The WMR is controlled to follow a reference trajectory⁷ with the control input

$$v_r = 1 \text{ m/s}, \omega_r = \begin{cases} 0.75 \text{ rad/s}, & \text{if } t < 17 \text{ s} \\ 0.75(18 - t) \text{ rad/s}, & \text{if } 17 \text{ s} \leq t \leq 18 \text{ s} \\ 0 \text{ rad/s}, & \text{if } t > 18 \text{ s}. \end{cases}$$

The initial conditions of the reference trajectory and the WMR are set to be $[x_r(0) \ y_r(0) \ \theta_r(0)]^T = [0 \ 0 \ \pi/4]^T$ and $[x(0) \ y(0) \ \theta(0)]^T = [3 - 2\pi]^T$, respectively. Both the disturbances $F(q)$ and τ_d are assumed to be $f_1 = f_2 = f_3 = v_c + \omega_c + 0.2$ and

$$\tau_{d1} = \tau_{d2} = \tau_{d3} = \begin{cases} \sin(t) + \cos(t), & \text{if } 0 \leq t < 10 \text{ s} \\ \sin(t) + \cos(t) + 3, & \text{if } t \geq 10 \text{ s}, \end{cases}$$

respectively. The linear velocity of the driving wheels is limited by $a = 3 \text{ m/s}$ and the half length of the wheelbase for the WMR is given by $d = 0.25$. Then, the diamond-shaped input constraint is given by $\mathbb{U}_c = \{|v_c|/3 + |\omega_c|/12 \leq 1\}$ with $b = a/d = 12$. For the outer loop optimization problem, the weighting matrices in the cost function are designed as $P = \text{diag}\{0.1 \ 0.1\}$ and $R = \text{diag}\{0.2 \ 0.4\}$ according to Lemma 1. The gains of the terminal controller in (28) are set to be $k_1 = k_2 = 1.5$. The prediction horizon and the sampling period are given as $T = 3 \text{ s}$ and $h = 0.01 \text{ s}$, respectively. For the inner loop system, by choosing the positive define gains β_{13} and β_{24} , the estimated velocities by the ESO can track the real velocities. The parameters of the ESO are set as $\beta_{13} = \text{diag}\{30 \ 30\}$ and $\beta_{24} = \text{diag}\{255 \ 255\}$. In addition, the gain for the nonlinear state error feedback controller is chosen as $k_\tau = \text{diag}\{20 \ 50\}$.

The simulation results are shown in Figure 3. The tracking performances of the WMR are plotted in Figures 3A and 3B. It is shown that, although there exist initial state errors, the WMR tracks the reference curve. Moreover, the error state q_e converges to zero. The optimal control signal u_c and the control torque τ are depicted in Figures 3C and 3D. It is shown that u_c and τ are limited by the input constraint (25). To evaluate the input constraint (25), the curve $|v_c|/a + |\omega_c|/b$ is presented in Figure 3E. It can be observed that the input constraint (25) is activated over the interval $t \in [0, 0.5] \text{ s}$. During this interval, the constraint for control signal u_c , ie, $u_c \in \mathbb{U}_c$, is also satisfied, which presents the satisfaction of the input constraint (25). In addition, the estimate values of the external disturbances \hat{w} are shown in Figure 3F. It is shown that the external disturbances are estimated well by the ESO.

5.2 | Double lane change trajectory test

The double lane change trajectory is defined as follows:

$$y_r(x) = \frac{4.05}{2} (1 + \tanh(z_1)) - \frac{5.7}{2} (1 + \tanh(z_2)),$$

$$\theta_r(x) = \arctan \left(4.05 \left(\frac{1}{\cosh(z_1)} \right)^2 \left(\frac{1.2}{25} \right) - 5.7 \left(\frac{1}{\cosh(z_2)} \right)^2 \left(\frac{1.2}{21.95} \right) \right),$$

where $z_1 = \frac{2.4}{25} (x - 27.19) - 1.2$ and $z_2 = \frac{2.4}{21.95} (x - 56.46) - 1.2$. It is obvious that both $y_r(x)$ and $\theta_r(x)$ are the nonlinear functions on x .

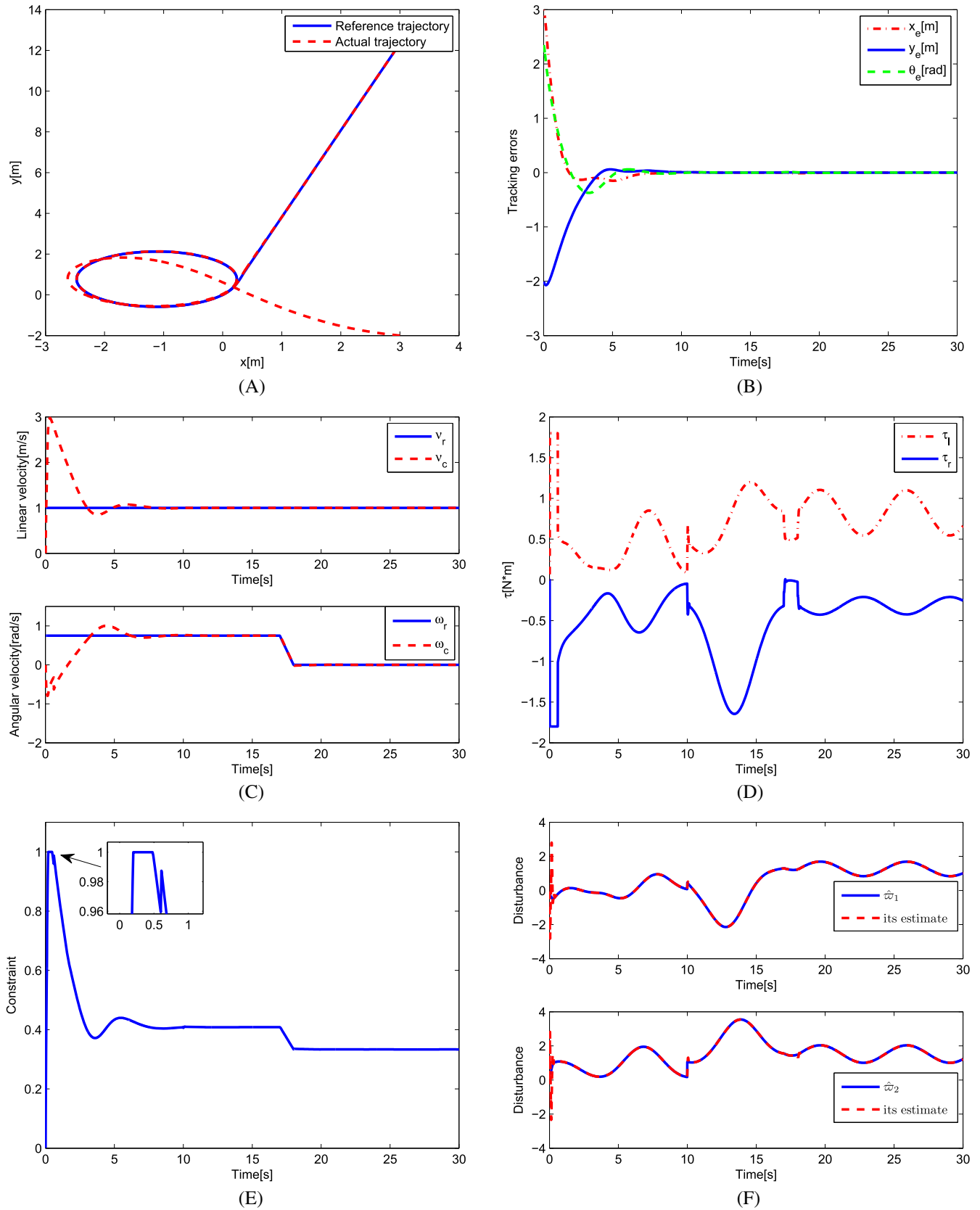


FIGURE 3 The performance of tracking a reference trajectory. A, Trajectory tacking; B, Trajectory tacking errors; C, Linear and angular velocities; D, Control torques; E, Constraint; F, Disturbance estimates [Colour figure can be viewed at wileyonlinelibrary.com]

The simulation results are shown in Figure 4. The trajectory tracking results of the double lane change trajectory are shown in Figures 4A and 4B. The real velocity η is presented in Figure 4C. The trajectory tracking errors are shown in Figure 4D. From the results in Figure 4, the WMR tracks the reference trajectory and the reference control inputs well, respectively. In addition, the simulation results of the previous work are found in the work of Yang et al.²² By comparing the errors in Figure 4D with the ones in the work of Yang et al.²² the maximal error in this paper is smaller than that in the aforementioned work.²² Finally, the sum-square error (SSE) for each component of the state-following error q_e is proposed to test the performance of trajectory tracking. The SSE in this paper is

$$SSE_1 = [0.0026 \ 0.0051 \ 0.0019]^T$$

and, in the previous work,²² it is

$$SSE_2 = [0.0142 \ 0.0312 \ 0.0024]^T.$$

It is shown that the SSE in this paper is smaller than that in the previous work.²²

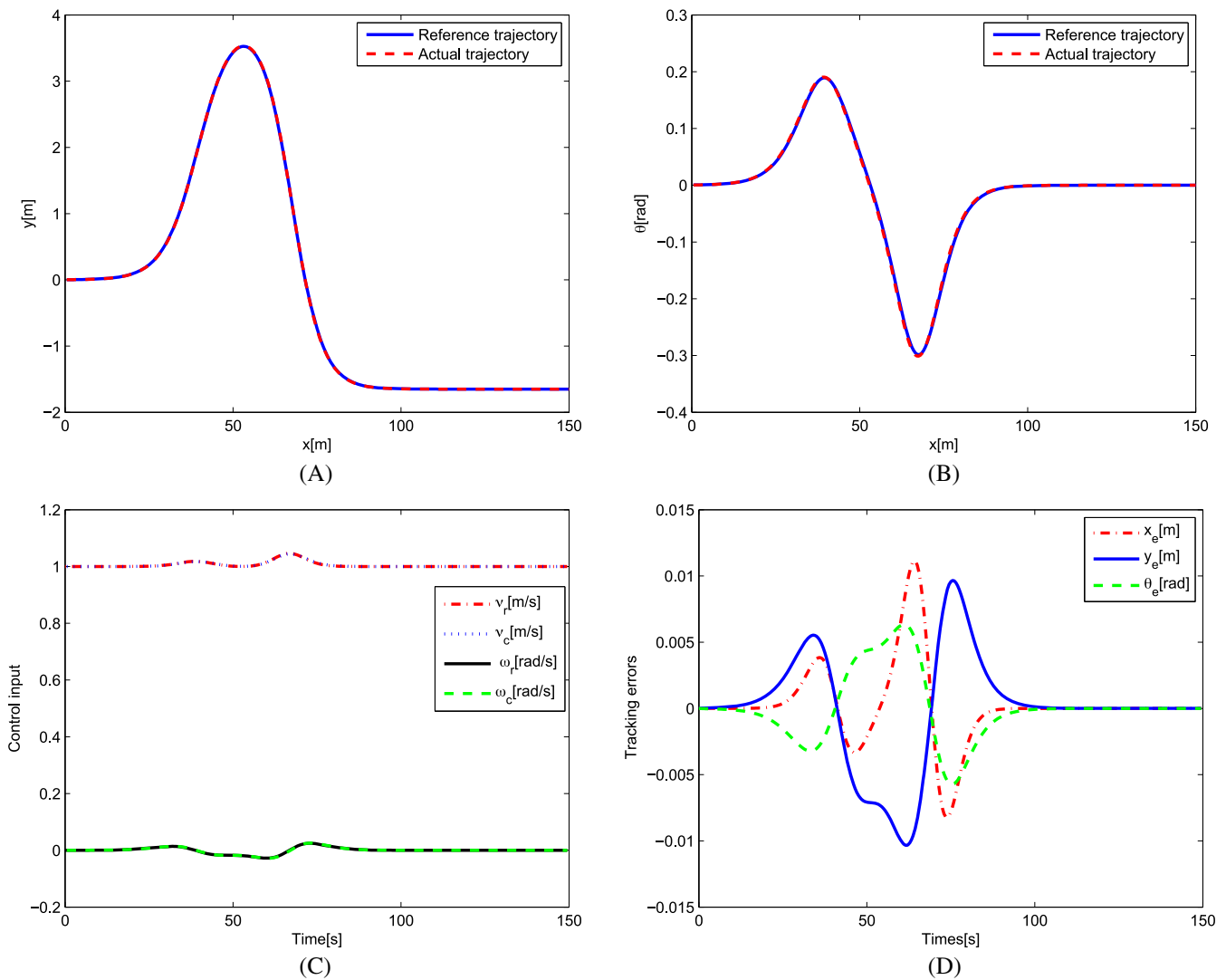


FIGURE 4 The performance of tracking a double lane change trajectory. A, Trajectory tracking of $y(x)$; B, Trajectory tracking of $\theta(x)$; C, Control input; D, Trajectory tracking errors [Colour figure can be viewed at wileyonlinelibrary.com]

5.3 | Parallel parking trajectory test

In order to present the docking performance, a parallel parking trajectory test is conducted for an initial pose $[x(0) \ y(0) \ \theta(0)]^T = [5, 3, \frac{3\pi}{4}]$. From the work of Lee et al,³⁵ the parallel parking trajectory is given as

$$x_r(t) = \begin{cases} 2a_0 \cos\left(c_0\left(t + \frac{\pi}{4c_0}\right)\right) + a_0\sqrt{2}, & 0 \leq t \leq \frac{\pi}{2c_0} \\ 0, & \frac{\pi}{2c_0} \leq t \end{cases}$$

$$y_r(t) = \begin{cases} b_0 \sin\left(2c_0\left(t + \frac{\pi}{4c_0}\right)\right) + b_0, & 0 \leq t \leq \frac{\pi}{2c_0} \\ 0, & \frac{\pi}{2c_0} \leq t \end{cases}$$

$$\theta_r(t) = \begin{cases} \pi - \tan^{-1}\left(\frac{b_0 \cos(2c_0(t + \pi/4c_0))}{a_0 \sin(c_0(t + \pi/4c_0))}\right), & 0 \leq t \leq \frac{\pi}{2c_0} \\ 0, & \frac{\pi}{2c_0} \leq t \end{cases}$$

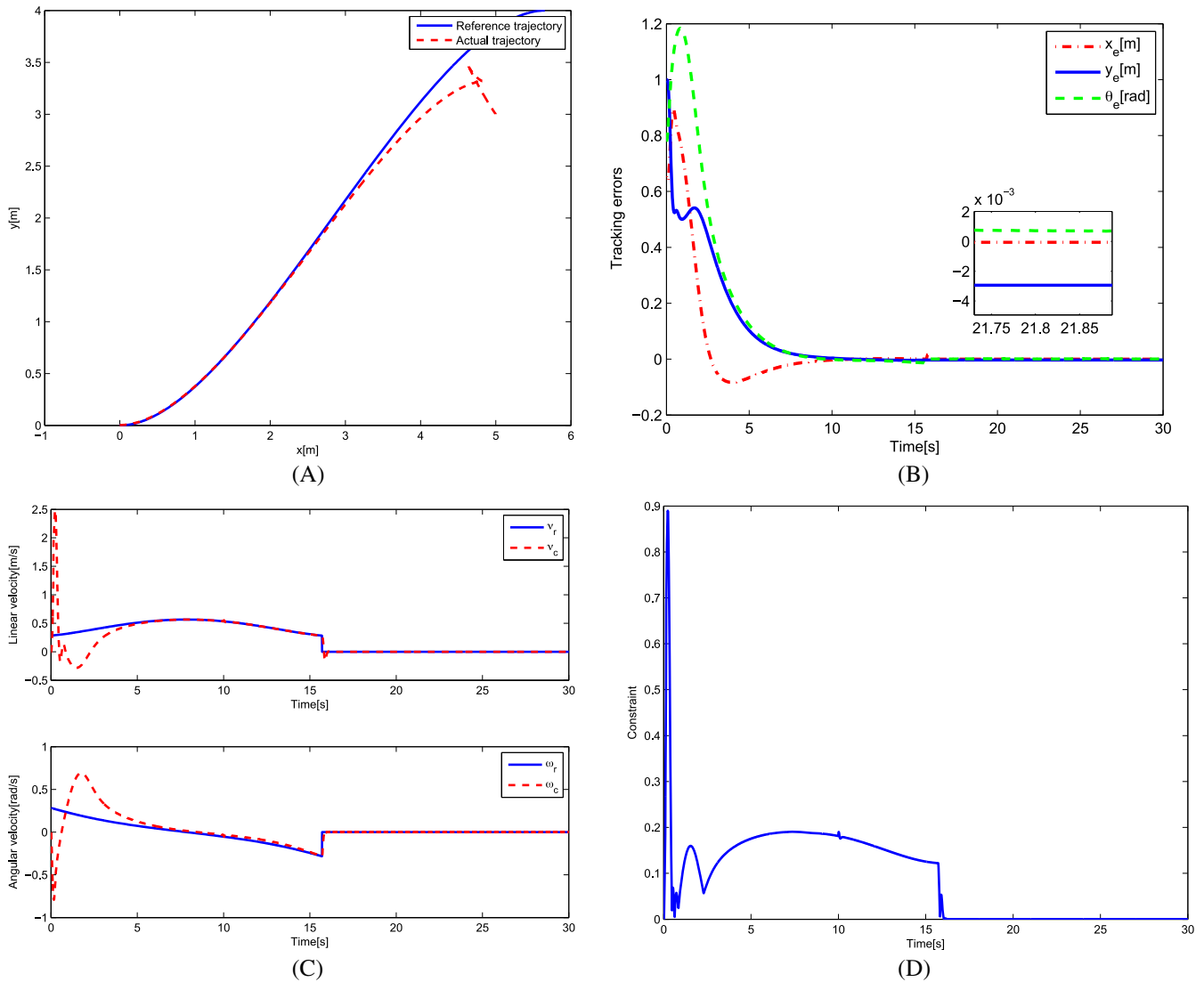


FIGURE 5 The performance of tracking parallel parking trajectory. A, Trajectory tacking; B, Trajectory tacking errors; C, Linear and angular velocities; D, Constraint [Colour figure can be viewed at wileyonlinelibrary.com]

$$v_r(t) = \begin{cases} 2c_0 \sqrt{a_0^2 \sin^2 \left(c_0 \left(t + \frac{\pi}{4c_0} \right) \right) + b_0^2 \cos^2 \left(2c_0 \left(t + \frac{\pi}{4c_0} \right) \right)}, & 0 \leq t \leq \frac{\pi}{2c_0} \\ \pi, & \frac{\pi}{2c_0} \leq t \end{cases}$$

$$\omega_r(t) = \begin{cases} \frac{a_0 b_0 c_0 \left(\cos \left(c_0 \left(t + \frac{\pi}{4c_0} \right) \right) \cos \left(2c_0 \left(t + \frac{\pi}{4c_0} \right) \right) + 2 \sin \left(c_0 \left(t + \frac{\pi}{4c_0} \right) \right) \sin \left(2c_0 \left(t + \frac{\pi}{4c_0} \right) \right) \right)}{\left(a_0 \sin \left(c_0 \left(t + \frac{\pi}{4c_0} \right) \right) \right)^2 + \left(b_0 \cos \left(c_0 \left(t + \frac{\pi}{4c_0} \right) \right) \right)^2}, & 0 \leq t \leq \frac{\pi}{2c_0} \\ 0, & \frac{\pi}{2c_0} \leq t, \end{cases}$$

where $a_0 = 2$, $b_0 = 2$, and $c_0 = 0.1$. The simulation results are shown in Figure 5. Tracking performance of the WMR is plotted in Figure 5A. The WMR controlled by the proposed controller tracks the parallel parking trajectory. The state errors are shown in Figure 5B. It demonstrates that the state errors using the proposed controller converge asymptotically to zero. The control input quantities are presented in Figure 5C. The linear velocity and the angular velocity track the given signals and stop at the final pose. The input constraint of $|v_c|/a + |\omega_c|/b \leq 1$ is shown in Figure 5D. It is shown that the linear velocity and the angular velocity satisfy the input constraint.

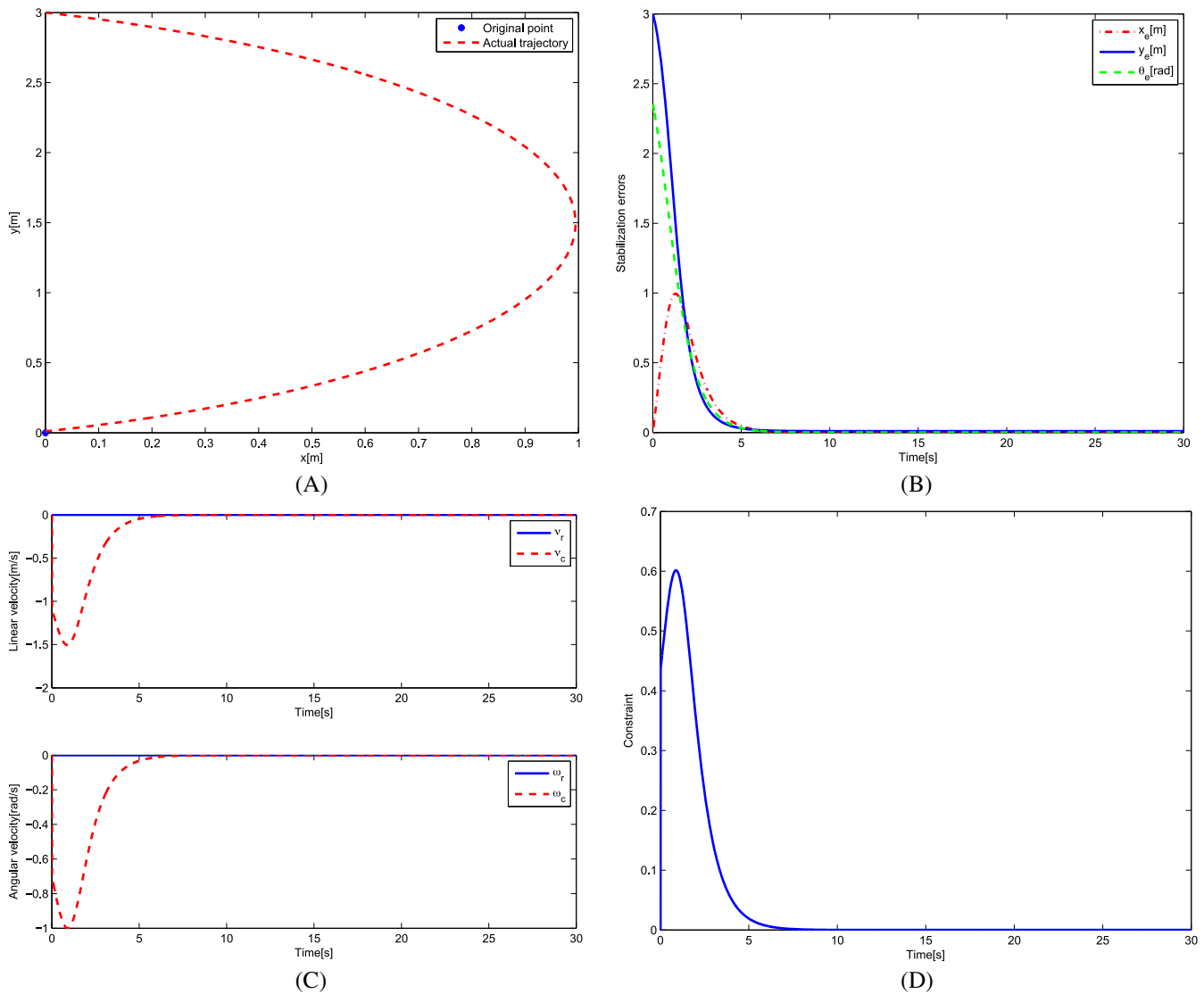


FIGURE 6 The performance of tracking a constant reference. A, Trajectory of the WMR; B, Stabilization errors; C, Linear and angular velocities; D, Constraint. WMR, wheeled mobile robot [Colour figure can be viewed at wileyonlinelibrary.com]

In addition, considering that the parallel parking with small lateral offset is hard to control, a constant reference is given to verify the performance under the proposed control scheme. Simulation is conducted for the initial pose $[x(0) \ y(0) \ \theta(0)]^T = [0 \ 3 \ \frac{3\pi}{4}]^T$ and a constant reference $[x_r(0) \ y_r(0) \ \theta_r(0)]^T = [0 \ 0 \ 0]^T$. The simulation results are shown in Figure 6. In Figure 6A, the WMR is driven to the desired position under the proposed controller. In Figure 6B, the stabilization errors tend to be zero finally. In Figure 6C, the linear velocity and angular velocity finally stabilize to 0 m/s and 0 rad/s, respectively. In Figure 6D, it is shown that the linear velocity and the angular velocity satisfy the input constraint $|v_c|/a + |\omega_c|/b \leq 1$. In conclusion, all of the simulation results verify the robustness and effectiveness of the proposed control strategy.

6 | CONCLUSION

A dual closed-loop control was presented for trajectory tracking of a WMR. The ADRC scheme with the ESO was proposed to estimate and compensate the external disturbances in the inner loop system. In the outer loop system, the MPC strategy was developed to generate the desired velocity, where the WMR is subject to a type of diamond-shaped input constraint. The stabilities for the dual closed-loop system and the recursive feasibility for the MPC scheme were achieved by the proposed control strategy. Finally, the robustness and effectiveness of the proposed control scheme were verified by simulations.

ACKNOWLEDGEMENTS

The authors would like to thank the anonymous reviewers for their detailed comments that helped to improve the quality of this paper. This work was supported by the National Natural Science Foundation of China under Grants 61973230, 61573301, and 61733012.

ORCID

Hongjiu Yang  <https://orcid.org/0000-0001-9343-8068>

Yuanqing Xia  <https://orcid.org/0000-0002-5977-4911>

REFERENCES

- Ren W, Atkins E. Distributed multi-vehicle coordinated control via local information exchange. *Int J Robust Nonlinear Control*. 2007;17:1002-1033.
- Wang P, Ding B. Distributed RHC for tracking and formation of nonholonomic multi-vehicle systems. *IEEE Trans Autom Control*. 2014;59(6):1439-1453.
- Simanek J, Reinstein M, Kubelka V. Evaluation of the EKF-based estimation architectures for data fusion in mobile robots. *IEEE/ASME Trans Mechatron*. 2015;20(2):985-990.
- de Wit CC, Sordalen OJ. Exponential stabilization of mobile robots with nonholonomic constraints. *IEEE Trans Autom Control*. 1992;37(11):1791-1797.
- Xiao H, Li Z, Chen CLP. Formation control of leader-follower mobile robots' systems using model predictive control based on neural-dynamic optimization. *IEEE Trans Ind Electron*. 2016;63(9):5752-5762.
- Lian C, Xu X, Chen H, He H. Near-optimal tracking control of mobile robots via receding-horizon dual heuristic programming. *IEEE Trans Cybern*. 2015;46(11):2484-2496.
- Huang D, Zhai J, Ai W, Fei S. Disturbance observer-based robust control for trajectory tracking of wheeled mobile robots. *Neurocomputing*. 2016;198:74-79.
- Lin WS, Yang PC. Adaptive critic motion control design of autonomous wheeled mobile robot by dual heuristic programming. *Automatica*. 2008;44(11):2716-2723.
- Song Y, Huang X, Wen C. Tracking control for a class of unknown nonsquare MIMO nonaffine systems: a deep-rooted information based robust adaptive approach. *IEEE Trans Autom Control*. 2016;61(10):3227-3233.
- Saradagi A, Muralidharan V, Krishnan V, Menta S, Mahindrakar AD. Formation control and trajectory tracking of nonholonomic mobile robots. *IEEE Trans Control Syst Technol*. 2018;26(6):2250-2258.
- Chen WH, Ballance DJ, Gawthrop PJ, O'Reilly J. A nonlinear disturbance observer for robotic manipulators. *IEEE Trans Ind Electron*. 2000;47(4):932-938.
- Song Y, Wang Y, Wen C. Adaptive fault-tolerant PI tracking control with guaranteed transient and steady-state performance. *IEEE Trans Autom Control*. 2017;62(1):481-487.
- Yang H, Fan X, Shi P, Hua C. Nonlinear control for tracking and obstacle avoidance of a wheeled mobile robot with nonholonomic constraint. *IEEE Trans Control Syst Technol*. 2016;24(2):741-746.

14. Han J. From PID to active disturbance rejection control. *IEEE Trans Ind Electron*. 2009;56(3):900-906.
15. Tian G, Gao Z. Frequency response analysis of active disturbance rejection based control system. Paper presented at: 2007 IEEE International Conference on Control Applications; 2007; Singapore.
16. Xia Y, Pu F, Li S, Gao Y. Lateral path tracking control of autonomous land vehicle based on ADRC and differential flatness. *IEEE Trans Ind Electron*. 2016;63(5):3091-3099.
17. Li J, Xia Y, Qi X, Zhao P. Robust absolute stability analysis for interval nonlinear active disturbance rejection based control system. *ISA Transactions*. 2017;69:122-130.
18. Zhao L, Yang Y, Xia Y, Liu Z. Active disturbance rejection position control for a magnetic rodless pneumatic cylinder. *IEEE Trans Ind Electron*. 2015;62(9):5838-5846.
19. Wu D, Chen K. Frequency-domain analysis of nonlinear active disturbance rejection control via the describing function method. *IEEE Trans Ind Electron*. 2013;60(9):3906-3914.
20. Zhao Z, Guo B. A nonlinear extended state observer based on fractional power functions. *Automatica*. 2017;81:286-296.
21. Mayne DQ, Rawlings JB, Rao CV, Scokaert POM. Constrained model predictive control: stability and optimality. *Automatica*. 2000;36(6):789-814.
22. Yang H, Guo M, Xia Y, Chen L. Trajectory tracking for wheeled mobile robots via model predictive control with softening constraints. *IET Control Theory Appl*. 2018;12(2):206-214.
23. Xiao H, Li Z, Yang C, et al. Robust stabilization of a wheeled mobile robot using model predictive control based on neurodynamics optimization. *IEEE Trans Ind Electron*. 2017;64(1):505-516.
24. Gu D, Hu H. Receding horizon tracking control of wheeled mobile robots. *IEEE Trans Control Syst Technol*. 2006;14(4):743-749.
25. Ma D, Xia Y, Li T, Chang K. Active disturbance rejection and predictive control strategy for a quadrotor helicopter. *IET Control Theory Appl*. 2016;10(17):2213-2222.
26. Chen X, Jia Y. Input-constrained formation control of differential-drive mobile robots: geometric analysis and optimisation. *IET Control Theory Appl*. 2014;8(7):522-533.
27. Sun Z, Xia Y. Receding horizon tracking control of unicycle-type robots based on virtual structure. *Int J Robust Nonlinear Control*. 2016;26(17):3900-3918.
28. Yu S, Li X, Chen H, Allgöwer F. Nonlinear model predictive control for path following problems. *Int J Robust Nonlinear Control*. 2015;25(8):1168-1182.
29. Kühne F, Lages WF, da Silva JG Jr. Model predictive control of a mobile robot using linearization. *Proc Mechatron Robotics*. 2004;4(4):525-530.
30. van Essen HA, Nijmeijer H. Non-linear model predictive control for constrained mobile robots. Paper presented at: 2001 European Control Conference (ECC); 2001; Porto, Portugal.
31. Fontes F. Discontinuous feedbacks, discontinuous optimal controls, and continuous-time model predictive control. *Int J Robust Nonlinear Control*. 2003;13(3-4):191-209.
32. Wächter A, Biegler LT. On the implementation of an interior-point filter line-search algorithm for large-scale nonlinear programming. *Mathematical Programming*. 2006;106(1):25-57.
33. Eele AJ, Richards A. Path-planning with avoidance using nonlinear branch-and-bound optimization. *J Guid Control Dyn*. 2015;32(2):384-394.
34. Falugi P, Kerrigan E, Wyk E. Imperial College London Optimal Control Software (ICLOCS). <http://www.ee.ic.ac.uk/ICLOCS/>
35. Lee TC, Song KT, Lee CH, Teng CC. Tracking control of unicycle-modeled mobile robots using a saturation feedback controller. *IEEE Trans Control Syst Technol*. 2001;9(2):305-318.

How to cite this article: Yang H, Guo M, Xia Y, Sun Z. Dual closed-loop tracking control for wheeled mobile robots via active disturbance rejection control and model predictive control. *Int J Robust Nonlinear Control*. 2019;1–20. <https://doi.org/10.1002/rnc.4750>